Numerical analysis of superoleophilic-superhydrophobic filtration system for emulsions separation using lattice Boltzmann method

Luma Al-Tamimi, Hassan Farhat

Numerical analysis of superoleophilic-superhydrophobic filtration system for emulsions separation using lattice Boltzmann method

Luma Al-Tamimi* and Hassan Farhat

Department of Mechanical Engineering,
Wayne State University,
5050 Anthony Wayne Dr., Detroit,
MI, 48202, USA
Email: et4700@wayne.edu
Email: av9328@wayne.edu
*Corresponding author

Abstract: A novel 3D hybrid quasi-steady thermal lattice is used to study the oil-water separation in stable emulsions and evaluate the efficiency of superoleophilic/superhydrophobic filtration systems through a variety of parameters. This work introduces the first 3D LBM model that combines the effects of surfactant and thermal conditions on the contact angle of a droplet adhering to a wall while accounting for all factors contributing to the complexity of emulsions systems. The LBM model demonstrated several key advantages: it mimics the superwetting filter system with any desired contact angle, evaluates wetting and oil-water separation under a broad array of conditions and increases the opportunity for innovation of superwetting filter designs by allowing modification and validation of various conditions. Furthermore, it is useful for highlighting the mechanisms that take place in the filtration process, such as the suspended phase behaviour, coalescence, and breakup, and determine which parameters can influence the greatest efficiencies.

Biographical notes: Luma Al-Tamimi received her PhD in Mechanical Engineering from the Wayne State University, MI, USA. She received her BS and MS in Automotive Engineering from the University of Windsor, Ontario, Canada. Her research interests focus on studying the rheological behaviour of oil in water emulsions under various conditions and the super-wetting filtration systems using a numerical simulation method called the lattice Boltzmann model (LBM). For the last ten years, she has been working at Ford Motor Company in different roles relating but not limited to design and release, feature software, and program management engineer.

Hassan Farhat received his MS and PhD in Mechanical Engineering from the Wayne State University, Detroit, Michigan, USA. During his PhD, he worked on numerical simulations of multiphase and multi-component fluids as a platform for the study of Colloidal suspensions using the lattice Boltzmann method (LBM). He is currently working as an engineering specialist in the Automotive Industry and Part-Time Faculty at the Wayne State University.

1   Introduction

The separation of oil and water in emulsions continues to be an obstacle in the oil production industry. The multiphase emulsion separators are typically the first unit of operations in the oil production line between reservoir and oil pipeline transportation (Oshinowo et al., 2015). Characteristically, crude oil emulsions are stable and challenging to separate. Therefore, the efficiency of oil/water separation technology plays a significant role in the economics of petroleum mining. Conventional separation methods such as gravity settling, centrifuges, ultrafiltration, gas flotation, oil skimmers, coalescers, magnetic separations, depth filters, and flotation technologies are suitable for immiscible oil-water mixtures but demonstrate less effectuality for emulsified oil-water mixtures, especially for surfactant-stabilised emulsions (Zhang et al., 2013; Cai

et al., 2015; Singh et al., 2021). Filtration membranes, although applied successfully in the separation of various emulsions, is an oil-water separation technique that presents limitations such as high energy consumption, modest absorption rates, low flux, and rapid permeation reduction caused by pore plugging by oil droplets, leading to drastic fouling issues (Padaki et al., 2015; Sadler and Crick, 2021).

It is of major scientific importance to conceive and engineer new filtration membrane materials to overcome the limitations of the conventional oil-water separation methods. Membrane materials that possess special wettability characteristics demonstrate superior advantages in the field of oil-water separation.

The most preferred method to measure surface wettability is the contact angle (θ), which can be described as the angle at the location whereby the tangential line along the liquid-air boundary intersects the solid-air or solid-liquid surface. Surfaces are categorised according to the value of their contact angle. For example, when the contact angle of a water droplet is very high ($\theta > 150°$), the surface can be classified as superhydrophobic. In contrast, a surface with deposited oil droplets exhibiting a very low contact angle ($\theta < 10°$) is classified as superoleophilic. With a smaller oil contact angle, the adhesive forces are significantly stronger than cohesive forces; therefore, the oil molecules interact more with solid molecules.

In the last decade, significant consideration has been given to super wetting membranes such as superhydrophobic/superoleophilic (SHO/SOI) (repels water and absorbs oil) or superhydrophilic/superoleophobic (SHI/SOO) (attracts water and repels oil). This is due to their effectual oil-water separation characteristics, cost-effectiveness, and environmentally friendly benefits. In further detail, the SHI/SOO surface displays considerable resistance to oil adhesion and a high affinity for water droplets, producing a low water contact angle. Comparatively, the SHO/SOI surface possesses a stronger attraction towards oil and a lower affinity for water droplets, leading to a higher water contact angle caused by the minimal surface energy (Rasouli et al., 2021).

Therefore, introducing these super wettability characteristics on the filter membrane materials can ameliorate the capability of oil-fouling resistance, recyclability, and filter efficiency in oil-water separation applications including but not limited to the oil refinery, treatment of oil-contaminated wastewater, and the removal of oil spills (Wu et al., 2020; Rasouli et al., 2021).

Feng et al. (2004) were the first to present a coated mesh film that concurrently demonstrated superhydrophobicity and superoleophilicity properties. Their experimental results indicate that the mesh film can successfully and efficiently separate oil/water mixtures. Thereafter, numerous researchers have focused on producing and designing SHO/SOI membranes using various fabrication methods. Of these studies, Tu et al. (2007) reported a facile one-step technique to prepare a SHO/SOI surface devoid of any chemical modification. The surface is generated via an air-brush method that sprays a polystyrene solution. The authors

stated that the air-brush method produced an excellent rough surface with a lower cost and separation efficiency of 95%. Moreover, Wang et al. (2009) demonstrated the production of a SHO/SOI copper mesh surface through a simple immersion process in nitric acid solution. The pore size influence on the wettability and mesh stability in acidic and salty solutions was studied. It was indicated that the wettability of the prepared mesh is stable in corrosive conditions. Additionally, Shang et al. (2012) described the creation of SHO/SOI membranes using a combination of electrospun and polymerisation as a fabrication method. Their experimental results showed that the prepared membranes displayed quick and effective separation for oil-water mixtures and decent stability towards a wide range of pH values. Afterward, Ju et al. (2015) claimed to follow a simple and economical preparation method to produce SHO/SOI polyvinylidene fluoride (PVDF) membranes through a solution immersion process. Their experimental findings demonstrate the oil droplet adhesion behaviour in contact with the PVDF. The images show the oil droplets spreading over the membrane due to the superoleophilic effect. Following those findings, Jiang et al. (2020) prepared a super-wetting nanofibres membrane with multi-stage roughness in one step by introducing SiO_2 nanoparticles into a PVDF spinning solution. The results demonstrated that the addition of SiO_2 nanoparticles changed the PVDF surface roughness and altered the wettability from hydrophobic to superhydrophobic. The results of the oil-water separation signify that the nanofibres membrane can successfully separate the oil-water mixture under the force of gravity and possess excellent chemical stability. Similarly, Wu et al. (2020) formulated a PVDF membrane that possessed SHI/SOO behaviour by adding $CaCO_3$ nanoparticles to modify roughness and attain low oil adhesion. Their experiments ensure that efficient oil/water separation can be attained by this membrane, given its anti-fouling performance, permeation flux, and filterisation of various emulsions. Furthermore, Woo et al. (2020) developed a superhydrophobic nanostructured glass microfibre membrane by using a vertical polymerisation composite coating method. It was reported that this modified membrane has excellent oil-water separation and chemical stability under corrosive acidic/alkaline solutions. Correspondingly, Singh et al. (2021) used kapok fibre as a coalescence filter for oil-water separation in an emulsion. They experimentally studied the oil-water separation efficiency of a prepared fibrous filter in terms of porosity, droplet size, and bed height. The experimental results indicated that the filter efficiency increased with porosity and bed height.

A thorough number of experimental studies have been conducted regarding the super-wetting membrane and its properties. Most experimental studies pertain to materials' fabrication and performance rather than the foundational mechanisms that facilitate oil/water separation. Experimental analyses are limited by feasible experimental setups, costly equipment, and the inability to accurately

represent all the parameters that affect super-wetting filter system performance.

In 2008, Varnik et al. used lattice-Boltzmann simulations to study the effects of abrupt changes in wettability on water/oil droplet motion during the separation of binary emulsion. A substrate was used composed of two halves, hydrophilic and hydrophobic, to represent the wetting gradient. The simulation results implied that the water component primarily drives the separation process due to water's strong propensity to wet the substrate's hydrophilic side and push away the other emulsion component to the hydrophobic side of the channel. Afterward, Darvishi and Foroutan (2016) numerically studied the hydrophobicity/oleophilicity properties of the PVDF membranes surface and its effectiveness as an oil-water separation method using molecular dynamic simulation. Oil and water molecules' mobility and adsorption mechanism on the hydrophobic surface was analysed. The simulation results revealed that water molecules formed in groups of four or greater possess higher mobility. Moreover, Mino et al. (2018) presented two-dimensional permeation simulations of an oil in water (O/W) emulsion that passes through fibrous hydrophilic filters using a free-energy lattice Boltzmann method (LBM). The impacts of the fibre diameter, filter porosity, and surface wettability on the droplets' coalescing performances were explored. Their simulation results indicate that the droplet coalescence rate rose with the increase of filter pore spacings, forming larger drops. However, the separation efficiency decreased, allowing more drops to pass through the filter. More recently, Gavazzoni et al. (2021) proposed a theoretical and a numerical model to predict the super-wetting behaviour on structured surfaces such as pillars and porous surfaces. The Monte Carlo four-spin cellular Potts model simulation results indicate that the hydrophobicity of the substrate controls the water behaviour. However, their simulation was unable to predict the oil behaviour, claiming that it is more complex due to the oleophilic effect on the surface.

Compared to the experimental advancements in the field, the numerical studies are lesser known. Ultimately, challenges remain in providing a deeper understanding of the super-wetting filtration system. Consequently, a greater focus must be placed on essential numerical research related to understanding the dynamic between oil, water, and surfaces. There is a need for more numerical analyses concerning the oil-water efficiency of superhydrophobic and superoleophilic membranes within the influence of several parameters. This is important in building a theoretical basis that can later be used for practical applications.

Among the various numerical simulation methods for studying droplet dynamics behaviour at pore scale in a multiphase and multi-component flows, the lattice-Boltzmann numerical simulation method displays the highest potential due to its accuracy, parallelism, capability of modelling complex geometries and stability for wide range of fluid properties (Al-Tamimi et al., 2021). Further

advantages of the LBM include the no-slip bounce-back boundary condition which allows the simulation of complex boundaries flows with little computational cost, the ability of dealing with non-uniform surface tension along the fluid-fluid interface, and the ability to track interfaces in multiphase flow at each time-step (Farhat et al., 2014).

Until now, no researchers have utilised LBM for analysing superoleophilic/superhydrophobic filtration systems. This research gap motivated us to use our novel-developed 3D model colour-gradient hybrid quasi-steady thermal lattice-Boltzmann model for evaluating the superoleophilic/superhydrophobic filtration of emulsions. This is the first 3D LBM model that combines the effects of surfactant and thermal conditions on the contact angle of a droplet adhering to a wall while accounting for all factors contributing to the complexity of emulsions systems. Moreover, the model is capable of handling multiphase fluids with density and viscosity differences.

A simple superoleophilic filtration element is placed in a rectangular duct, through which O/W emulsion is flown with variety of volume fractions, droplets' size, and suspended phase spatial distribution to assess the efficiency of the filtration element. The LBM simulation results present the behaviour of the droplet, as it attaches to and spreads when in contact with the super-wetting filter type.

The key advantage of this LBM model is that it mimics the super-wetting filter system with any desired contact angle. Furthermore, this LBM model can successfully evaluate wetting and oil-water separation phenomena under a broad range of parameters and conditions. The LBM model presented in this work can simulate the droplet dynamics behaviour passing through a superoleophilic-superhydrophobic filter and is proven to be capable of demonstrating the complexity of the oil-water separation dynamics. Additionally, the LBM model improves the oil-water separation efficiency by increasing the innovation opportunity of designing new super-wetting filters. The wetting parameters can be accordingly modified and validated under various conditions.

Although several experimental works focus on superoleophilic-superhydrophobic filtration, using this LBM numerical study will be useful in highlighting the mechanisms that take place in the filtration process, leading to high efficiencies such as the suspended phase adhesion behaviour, its coalescence, and break-up.

2 Numerical method

2.1 The lattice Boltzmann model

The three-dimensional (3D) lattice Boltzmann colour-gradient model is applied in this work. The model used $f_i^{L,H}$ to represent the distribution function for the immiscible fluids (light and heavy), where $i = 0, \ldots, 18$ for 3DQ19 lattice velocity vectors, as shown in Figure 1. Then the total density distribution function given by $f_i = f_i^L + f_i^H$. The single relaxation

Bhatnagar-Gross-Krook (BGK) collision operator is the most prevalent model for the lattice Boltzmann equation, composed of three steps: the collision step, re-colouring step, and streaming step. The collision step is calculated as follows:

$$\hat{f}_i^q(x, t+\delta_t) = f_i^q(x, t) - \frac{1}{\tau^q}$$
$$\times \left[f_i^q(x, t) - f_i^{q,eq}(\rho, \rho u) \right] + \phi(x), \tag{1}$$

where $f_i^q(x, t)$ is the distribution function at the position x and time t in the ith velocity direction, q represents the light and heavy fluids, δ_t is the lattice time step, f^{eq} is the equilibrium distribution function, and $\phi_i(x)$ is the source term. From the distribution functions, the macroscopic density $\rho = \sum_{i=0}^{Q-1} f_i^{eq}$ and momentum $\rho u = \sum_{i=1}^{Q-1} c_i f_i^{eq}$ are determined. The variable fluids are collided individually to simulate a high-density ratio within the colour-gradient LBM using the equilibrium distribution functions given below (Farhat et al., 2011):

$$f_i^{L,eq} = \rho^L \omega_i \left[1 + \frac{3}{c^2} c_i \cdot u + \frac{9}{2c^4}(c_i \cdot u)^2 - \frac{3}{2c^2} u \cdot u \right]$$
$$f_i^{H,eq} = \rho^H \omega_i \left[r_i + \frac{3}{c^2} c_i \cdot u + \frac{9}{2c^4}(c_i \cdot u)^2 - \frac{3}{2c^2} u \cdot u \right], \tag{2}$$

where ρ^L, ρ^H are the density of the light and heavy fluids respectively, $c_i = e_i/\delta_t$ is the lattice velocity in the ith direction, u is the local fluid velocity, $c = \delta_x/\delta_t$, $c_s = c/\sqrt{3}$ is the lattice speed of sound, and ω_i are the lattice links weighting factors for the D3Q19 model $\omega_0 = 1/3$, $\omega_{1-2,4-6,8,10-11,13-15,17} = 1/36$, $\omega_{3,7,9,12,16,18} = 1/18$. The constant r_i is given by $r_{i \neq 0} = \gamma$ or $r_{i=0} = 2.25 - 1.25\gamma$, where $\gamma = \frac{\rho^L}{\rho^H} = \frac{(c_s^H)^2}{(c_s^L)^2}$ is the dimensionless density ratio. Then the kinematic viscosity is obtained from the relaxation time τ and speed of sound as follow $v = (\tau - 0.5)c_s^2\delta_t$.

The phase field function $\rho^N(x, t)$ is applied to track the interface between the two fluids (light and heavy) as follows:

$$\rho^N(x, t) = \frac{\rho^L(x, t) - \rho^H(x, t)}{\rho^L(x, t) + \rho^H(x, t)}$$
$$\rho^L(x, t) = \sum_0^{Q-1} f_i^L(x, t); \rho^H(x, t) \tag{3}$$
$$= \sum_0^{Q-1} f_i^H(x, t).$$

Then after the collision step, the fluids are segregated, and the following re-coloured (red and blue) distribution function equations are implemented to represent the segregation step (D'Ortona et al., 1995; Halliday et al., 2007):

$$\overline{\overline{R}}_i(x, t+\delta_t) = \frac{R}{R+B} \hat{f}_i(x, t+\delta_t)$$
$$+ \beta \frac{RB}{R+B} \omega_i \cos(\theta_f - \theta_i)|c_i|$$
$$\overline{\overline{B}}_i(x, t+\delta_t) = \frac{B}{R+B} \hat{f}_i(x, t+\delta_t)$$
$$- \beta \frac{RB}{R+B} \omega_i \cos(\theta_f - \theta_i)|c_i|, \tag{4}$$

where $\overline{\overline{R}}_i$, $\overline{\overline{B}}_i$, $\hat{f}_i$ are the post-collision post-segregation for red, blue, and total distribution functions respectively. θ_f and θ_i are the polar angle of the colour gradient and the angle of the velocity link respectively, and β is the segregation parameter for representing the interface thickness.

Following the segregation step, the streaming phase occurs, where the red and blue distribution functions propagate separately to the neighbouring lattice nodes as follows:

$$R_i(x + c_i\delta_t, t+\delta_t) = \overline{\overline{R}}_i(x, t+\delta_t)$$
$$B_i(x + c_i\delta_t, t+\delta_t) = \overline{\overline{B}}_i(x, t+\delta_t). \tag{5}$$

The contact angle for the suspended and suspending fluids in this LBM model is controlled by applying the fluid-solid interaction force on both fluids' nodes that are adjacent to the channel walls as follows (Martys and Chen, 1996):

$$N^{R,B}(x, t) = -\rho^{R,B}(x, t) \sum_{i=0}^{Q-1} \omega_i G_{ads}^{R,B} S(x + c_i\delta_t) c_i, \tag{6}$$

where $S(x + c_i\delta)$ can only have a value of one for the solid node or zero for the fluid node. $G_{ads}^{R,B}$ is a constant for the fluid-solid adhesion forces, which hold a negative value for wetting fluid and positive for non-wetting fluid.

2.2 The quasi-steady thermal model

The energy equation can be written after some mathematical simplification as follows:

$$\partial_t T + D_1 \partial_x T + D_2 \partial_y T + D_3 \partial_z T + D_4 T$$
$$+ D_5 \partial_{xx}^2 T + D_6 \partial_{yy}^2 T + D_7 \partial_{zz}^2 T + D_8 = 0.$$
$$D_1 = u_x; D_2 = u_y; D_3 = u_z;$$
$$D_4 = \partial_x u_x + \partial_y u_y + \partial_z u_z;$$
$$D_5 = D_6 = D_7 = -D_{ifs}; \tag{7}$$
$$D_8 = -\frac{\mu}{\rho c_p} \left[2(\partial_x u_x)^2 + 2(\partial_y u_y)^2 \right.$$
$$+ 2(\partial_z u_z)^2 + (\partial_x u_y + \partial_y u_x)^2$$
$$+ (\partial_y u_z + \partial_z u_y)^2 + (\partial_z u_x + \partial_x u_z)^2$$
$$\left. - \frac{2}{3}(\partial_x u_x + \partial_y u_y + \partial_z u_z)^2 \right];$$

where u_x, u_y, u_z are the fluid velocity components, μ is the dynamic viscosity and D_{ifs} is the thermal diffusivity.

2.3   The surfactants model:

In the 3D domain, the surfactant convection-diffusion equation is discretised, and after some mathematical manipulation, the following simplified equation is obtained:

$$\partial_t \Gamma + C_1 \partial_x \Gamma + C_2 \partial_y + C_3 \partial_z + C_4 \Gamma$$
$$+ C_5 \partial_{xx}^2 \Gamma + C_6 \partial_{yy}^2 \Gamma + C_7 \partial_{zz}^2 \Gamma + C_8 \partial_{xy}^2 \Gamma \qquad (8)$$
$$+ C_9 \partial_{xz}^2 \Gamma + C_{10} \partial_{yz}^2 \Gamma = 0.$$

The coefficients C_j are expressed as follows:

$$C_1 = u_{sx}; \; C_2 = u_{sy}; \; C_3 = u_{sz};$$
$$C_4 = \left(n_y^2 + n_z^2\right)\partial_x u_{sx} + \left(n_x^2 + n_z^2\right)\partial_y u_{sy} + \left(n_x^2 + n_y^2\right)\partial_z u_{sz}$$
$$-n_x n_y \left(\partial_y u_{sx} + \partial_x u_{sy}\right) - n_x n_z \left(\partial_z u_{sx} + \partial_x u_{sz}\right)$$
$$-n_y n_z \left(\partial_z u_{sy} + \partial_y u_{sz}\right) + \left(K u_x n_x + K u_y n_y + K u_z n_z\right);$$
$$C_5 = \left(n_x^2 - 1\right)D_s; \; C_6 = \left(n_y^2 - 1\right)D_s; \; C_7 = \left(n_z^2 - 1\right)D_s;$$
$$C_8 = 2n_x n_y D_s; \; C_9 = 2n_x n_z D_s; \; C_{10} = 2n_y n_z D_s;$$

where u_{sz}, u_{sy}, u_{sz} are the tangential velocity components and n_x, n_y, n_z are the components of the normal to the interface.

Figure 1   3DQ19 lattice velocity vectors
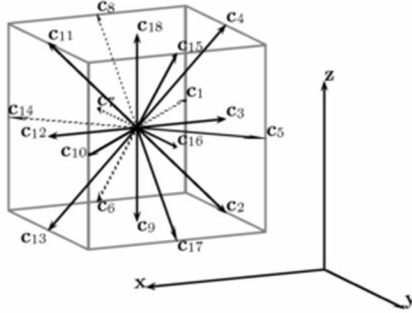
3   Model validation

We previously validated the developed two-dimensional hybrid lattice Boltzmann model with experimental results (Al-Tamimi et al., 2021). To validate the 3D LBM contact angle model, the simulation results were compared with the experimental work of Hou et al. (2018) and the previous 2D model results that have already been validated.

The experimental work used non-ionic surfactant TX-100, to replicate the experimental conditions and the properties of this type of surfactant, a relaxation time $\tau = 0.595$ was used and lead to kinematic viscosity $v_R = 2.78$ lu^2/ts for the suspended fluid (red fluid) and $v_B = 0.0317$ lu^2/ts for the suspending fluid (blue fluid). As a result, a viscosity ratio of $v_R/v_B = 86.26$ is obtained. Additionally, the following dimensionless parameters are used to matched those used by the 2D validation work such as dimensionless diffusion coefficient $D_s \approx 1.23 \times 10^{-2}$ lu^2/ts, elasticity $E_0 = 0.313$, interfacial tension $\sigma = 0.008$ lf/lu, gravity $g = 4.55 \times 10^{-6}$ lu/ts^2, bond number $Bo = 30.64$, and average density ratio between the two fluids was set to $\rho_R/\rho_B = 0.82$. For more in-depth details about the

reasoning of selecting these conditions, the reader is referred to the article of Al-Tamimi et al. (2021).

Then droplet with radius $R_d = 15[lu]$ was placed on the upper surface of a 3D domain with dimensions $210 \times 51 \times 35$ [lu^2]. A reference contact angle of 1,340 was applied to match the experimental contact angle for the case of clean droplets. Next the surfactant surface concentration was changed incrementally $\Gamma^* = 0 \rightarrow 0.9$, and the resultant static contact angles were measured from the simulation.

Figure 2 demonstrates the comparison between the 3D simulation results for sessile droplets that placed on an oil-wet surface, our previous 2D simulation results, and the results published by Hou. It is noticeable that the 3D simulation results match well the 2D results with improved outcome compared to the 2D results, which is expected since the 3D simulation is a more realistic representation of the physical case. The discrepancy in the results at higher concentrations may have been caused by the assumption in the surfactants and wettability alteration models.

Figure 2   Validation of the LBM model (see online version for colours)
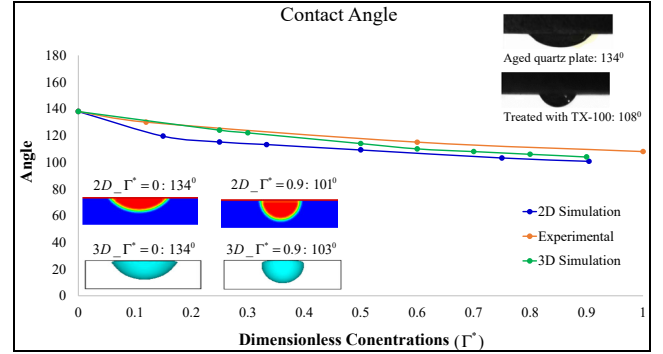
Notes: The top-right insets are from the experimental results (Hou et al., 2018) and the bottom-left inserts are the phase field contours from the 2D results (Al-Tamimi et al., 2021) and our current 3D simulations.

4   Simulation and discussion

The LBM model is utilised to study the emulsion rheology of oil-water separation and to evaluate the efficiency of superoleophilic-superhydrophobic filtration systems through various parameters such as droplet size, spatial distribution effect and volume fraction. In the subsequent simulations, 3D computational domains consisting of $161 \times 81 \times 61$ [lu^3] and $301 \times 81 \times 61$ [lu^3] are employed to simulate the permeation and separation of O/W emulsions passing through a modelled filter that possesses special wettability characteristics.

The filter was three-dimensionally modelled as a mesh consisting of vertical and horizontal rectangular solid walls crossing each other and representing a micro-section from the larger scale super-wetting filter mesh, as shown in Figure 3(a). Figure 3(a) also demonstrates the filter's dimensions in the front view, wherein the wall thickness is 4 [lu]. The filter consists of two layers of super-wetting

walls having separation distance of 20 [*lu*] to model the micro mesh as shown in Figure 3(b). The first layer is modelled as one vertical and horizontal wall, while the second layer is formed as one horizontal and two vertical walls, as shown in Figures 3(a) and 3(b).

To represent O/W emulsion, the oil droplets were positioned before the filter, while the entire domain was occupied with water as shown in Figure 3(b). The contact angle of the oil was set to 8° to simulate the superoleophilic-superhydrophobic filter system and thus obtain the superoleophilic wettability behaviour. The desired contact angle for suspended and suspending fluids is obtained through the $G_{ads}^{R,B}$ in equation (6). The reduction in contact angle can be achieved by increasing the negative value of G_{ads}^{R} and positive value of G_{ads}^{B}, leading to higher surface wettability behaviours, an increase in adhesion force, and greater droplet spreading.

Figure 3   (a) Graphic representation of the modelled superoleophilic-superhydrophobic filter (b) Simulation domain dimensions and geometric parameters (see online version for colours)

(a)

(b)
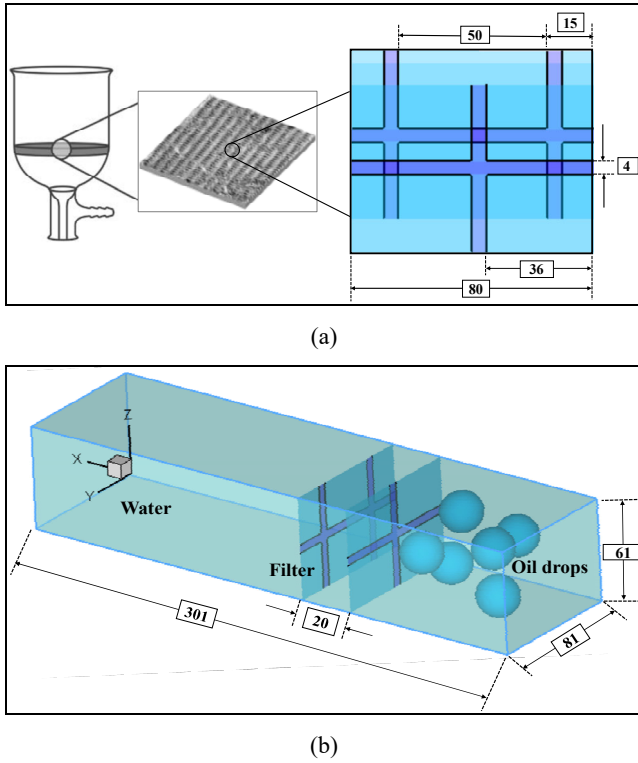
Notes: *on the left, a macro image of the filter (Mehanna and Crick, 2020). On the right side, an expanded portion of the filter revealing the modelled lattice structure from the front view.
**all dimensions are in the lattice unit.

Oil-water separation and effectiveness using the superoleophilic/superhydrophobic filter was analysed using a variety of parameters, including droplets' volume fraction, size, and location in the channel.

A source term $F = \dfrac{\Delta p}{\ell} = 7.5 \times 10^{-6}$ was applied to the fluid to induce a constant pressure gradient per unit length, experiencing a flow originating from the right boundary side and exiting through the left boundary. Subsequently, the periodic boundary condition was imposed on the inlet and outlet sides of the channel.

A variety of physical properties were employed in the simulation process, namely a relaxation time $\tau = 0.583$ for the suspending fluid (water) producing a kinematic viscosity $v_w = 0.0277 \ lu^2/ts$, and $\tau = 8.716$ for the suspended fluid (oil) resulting in $v_{oil} = 18.72 \ lu^2/ts$. Furthermore, the average density ratio and viscosity ratio between the oil and water is calculated to be 0.885 and 674.75, respectively.

The filter porosity ε_P, which is the measure of the void space in the filter medium, is calculated to be 93.2% as follows:

$$\varepsilon_P = \frac{V_p}{V_t} \cdot 100\%, \tag{9}$$

where V_p is the volume of the pore space and V_t is the volume of the whole filter structure.

The flux (J) for the fluid passing through the filter was determined according to the following equation (Wu et al., 2020):

$$J = \frac{V_o}{A\Delta t}, \tag{10}$$

where V_o is the volume of filtrate (oil droplet), Δt is the simulation time during the separation, and A is the frontal area of the oleophilic-hydrophobic filter, which is modelled using rectangular shapes, as shown in Figure 3(a).

Moreover, the filter efficiency (F_{eff}) is computed by evaluating the oil droplet volume before and after the oil-water separation process as follows (Sadler and Crick, 2021):

$$F_{eff} = \frac{V_{oil\_in} - V_{oil\_out}}{V_{oil\_in}} 100\%. \tag{11}$$

A dimensionless methodology is used for the analysis of the simulation parameters and results. The middle pore in the second layer of the filter, 50 *lu*, is used as a characteristic radius to obtain the dimensionless oil droplet radii (R_{d-s}), as shown in Figure 3(a). Then to normalise the time, the inverse shear strain rate $\dot{\gamma}_{H/4}^{-1} = 561$ is used as a characteristic time, which is determined at $H/4$ of the channel height (H) as hereby given (Al-Tamimi et al., 2021):

$$\dot{\gamma}_{H/4}^{-1} = \frac{H}{4u_{o@H/4}}, \tag{12}$$

where $U_{o@H/4}$ is the horizontal central velocity of the undisturbed parabolic flow computed at 1/4 channel height. Then MATLAB is used to solve the following velocity equation U_o (Delplace, 2018):

$$U_{o@z}(x,y) = \frac{16a^2}{\mu\pi^3}\frac{\Delta p}{\ell}\sum_{n=1}^{\infty}(-1)^{(n-1)}$$

$$\left[1 - \frac{\cosh\left(\frac{(2n-1)\pi y}{2a}\right)}{\cosh\left(\frac{(2n-1)\pi b}{2a}\right)}\right]\frac{\cos\left(\frac{(2n-1)\pi x}{2a}\right)}{(2n-1)^3}. \tag{13}$$

The simulations were achieved using the Linux operating system and a code written in the C programming language, all compiled using Intel (ICC).

4.1 Effect of droplets size distribution on the efficiency of the oleophilic-hydrophobic filters

Understanding the influence of oil droplet size on the oil-water separation performance is a critical requirement in designing and fabricating a practical separator filter. This section simulates the evolution of different oil droplet sizes during the oil-water separation. The droplet dimensionless radius is set to R_{d-s} = 0.12, 0.14, 0.16, 0.18, 0.2 to evaluate the effects of oil droplet size on the efficiency of the superoleophilic/superhydrophobic filter.

To obtain the same initial flux with the varying oil droplet radius size, the volume fraction must remain constant by modifying the quantity of the droplets in correlation with the droplet size, as shown in Table 1. As the radii decrease, the quantity of droplets increases from 6 drops to 28 drops to retain a constant volume fraction.

Figure 4 illustrates the time-dependent change in the morphology of the oil droplet during the separation process, using the superoleophilic/superhydrophobic filter for droplets with radius R_{d-s} = 0.2 and domain 161 × 81 × 61 [lu^3]. As the droplet contacts the filter, the oleophilic effect causes it to propagate around the filter, taking the shape of the filter walls as shown at the dimensionless time step t = 18 – 25. As more droplets approach the filter, the oil droplets coalesce and spread along the filter wall. The filter walls begin to swell in thickness due to an increase in droplets' coalescence and adhesion on the filter. The high effectiveness of this filter is displayed at t = 71, wherein it appears that the oil drops become entrapped by the first layer of the filter. Although the adhesion of oil on the filter walls is most effective during this oil-water separation technique, the break-up of droplets occurs nonetheless. Some oil droplets break up into smaller daughter droplets, which manage to pass through the first and second filter walls, as shown in t = 25 – 71, thus reducing the filter efficiency.

Figure 5 displays the filter efficiency of various sizes of oil droplets. With the increase in droplet size, the superoleophilic/superhydrophobic filter efficiency increases correspondingly. The positive correlation here matches the performance of most commercially available filters and corroborates other researchers' results (Bothamley, 2013; Oshinowo et al., 2015; Fan, 2016; Zhang et al., 2022).

In the case of the oil droplets with radius R_{d-s} < 0.2, it is noted that as the droplet size decreases, the droplet evolution increases along with the prevalence of

coalescence, as shown in Figure 6. Aside from the droplet's spatial distribution, the other factors that accelerate droplet evolution and coalescence at the early stages of the simulation are the high source term and low surfactant concentration (Oshinowo et al., 2015).

Even though some of the droplet's shapes evolved quickly at the start of the simulation to create larger droplets, the efficiency of the filter still decreased. In general, the generation of a larger droplet indicates an increased efficiency. In this case, however, the efficiency was not dramatically affected due to the other small droplets' locations and quantities. Before the large droplets attach to the wall, the smaller droplets first attach to the wall at the beginning of the simulation. Due to the droplets' small size and strong adhesion force caused by the superoleophilic effect, the droplets attach partially to the wall and the rest of the droplet break down into tiny drops as displayed in Figure 7. These miniscule droplets can escape from the filter walls, thus decreasing the filter efficiency. The larger, evolved droplets are able to fully attach to the wall, however, depending on their location, they may only achieve partial attachment.

Table 1   Droplet size vs. quantity for constant volume fraction

Volume fraction = 5.1%					
Droplets radius (dimensionless)	0.12	0.14	0.16	0.18	0.2
Droplets quantity	28	17	12	8	6

Figure 4   Oil droplet behaviour during the oil-water separation process with different dimensionless time steps (t) (see online version for colours)
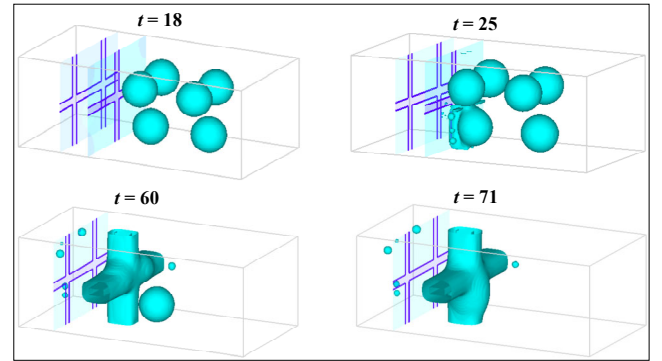
Additional simulation trials are performed to determine the smallest droplet size that can pass through the filter without contacting the wall. The larger domain 301 × 81 × 61 [lu^3] was used in this simulation to show how the droplets can pass the filter walls. As demonstrated in Figure 8, droplets with R_{d-s} = 0.08 can traverse both filter walls. This dimensionless radius is obtained by normalising the radius with the central pore of the filter's second layer, 50 lu. Consequently, filter structures should be designed to relegate droplets larger than R_{d-s} = 0.08 relative to the largest pore space or design micro-structured walls that can accommodate droplet distribution variance, so that droplets cannot pass through and remain attached to the filter walls.

Figure 5 The simulation results of the superoleophilic/ superhydrophobic filter efficiency with respect to oil droplets sizes (see online version for colours)
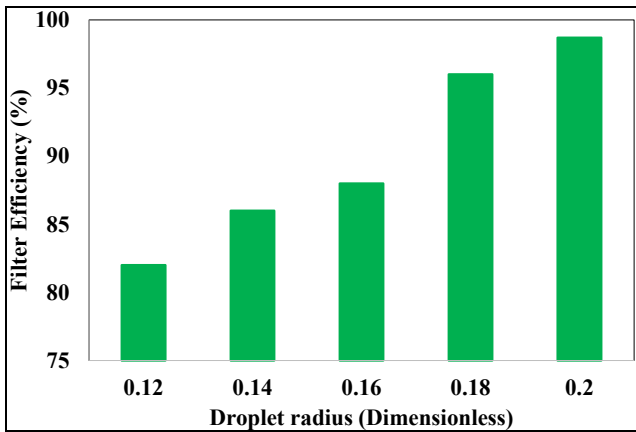
Figure 6 Effect of oil droplet radius on the droplet evolution for the modelled superoleophilic/superhydrophobic filter at dimensionless time step $t = 10$ (see online version for colours)
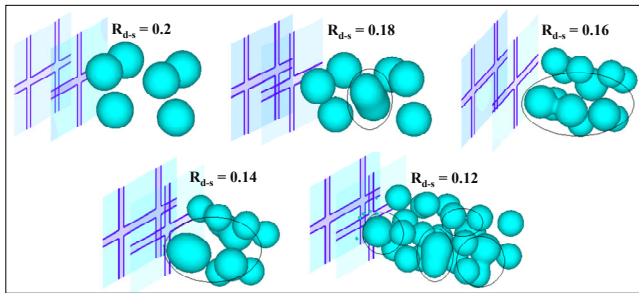
Figure 7 Illustration of oil-water separation mechanism for cases that leads to low super-wetting filter efficiency (see online version for colours)
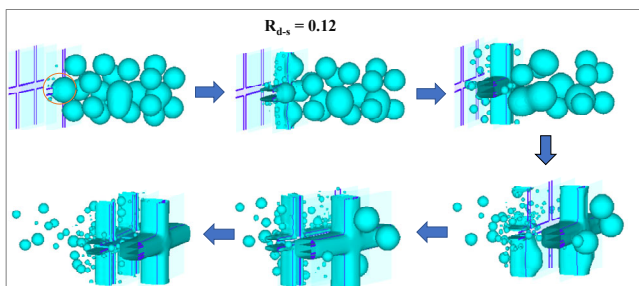
Oily water separators in all forms possess numerous limitations based on the droplet size that they can manage. It can be concluded that the effectiveness of the oily water separator depends on the size of the oil droplet. With smaller oil droplet sizes, the filter must be more effective. Larger droplets deposit on the filter walls more quickly and swell the wall thickness such that other droplets attach to the wall more easily.

Figure 8 Illustration of the smallest droplet size that can pass through the filter membrane (see online version for colours)
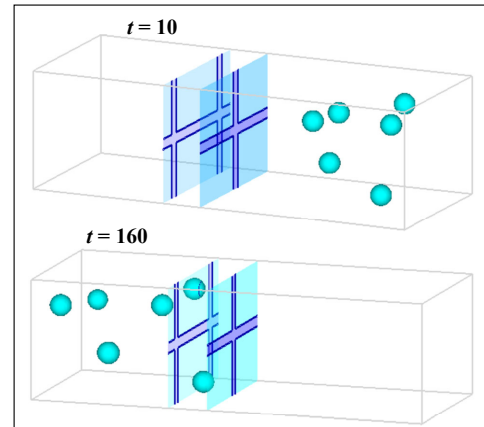
4.2 Influence of spatial distribution on the efficiency of oleophilic-hydrophobic filters

Another key factor in determining the performance of oil-water separation processes is the oil droplets' spatial distribution. In the following simulations a variety of dimensionless droplets radii (R_{d-s} = 0.16 and 0.2) were employed with random spatial distributions. In the case of R^{d-s} = 0.2, droplets with an organised distribution, possessing relatively equal spatial distribution, yielded a filter efficiency of 99%, as shown in Figure 9(a) left side. However, when the droplets were scattered in more arbitrary distributions, the efficiency value was reduced to 92% as shown in Figure 9(a) right side graph. Furthermore, with the case of smaller radii sizes, such as R_{d-s} = 0.16, it is noted that the randomisation of the droplet distribution for smaller droplets further exacerbates the discrepancy in efficiency values, as shown in Figure 9(b), where the filter efficiency for this radius decreased from 88% to 45%. This suggests that droplet distribution becomes more essential when droplet scattering rate decreases, leading to lower filter efficiency.

The behaviour of the droplets can explain the decrease in the filter efficiency as they spread further apart from each other. Droplets with smaller radii struggle to fully settle on the filter wall, as the probability of their affixation to the wall is decreased due to their smaller size. Consequently, they attach partially to the first filter wall, causing droplet break-up into smaller daughter droplets. These smaller new droplets may attach fully or partially to the second filter layer. If the daughter droplets attach partially to the second filter layer, another round of breakage will occur in the droplets and create even smaller droplets. The detached parts of the droplets manage to get through the filter walls as they have now split into smaller droplets and reduce the filter efficiency as shown in Figure 9(b).

Figure 9   Effect of oil droplets' spatial distribution on the oil-water separation efficiency, left side displays organised droplet distribution; right side shows scattered droplet distribution, (a) for the case of droplet radius $R_{d-s} = 0.2$ (b) for droplet radius $R_{d-s} = 0.16$ (see online version for colours)

(a)

(b)
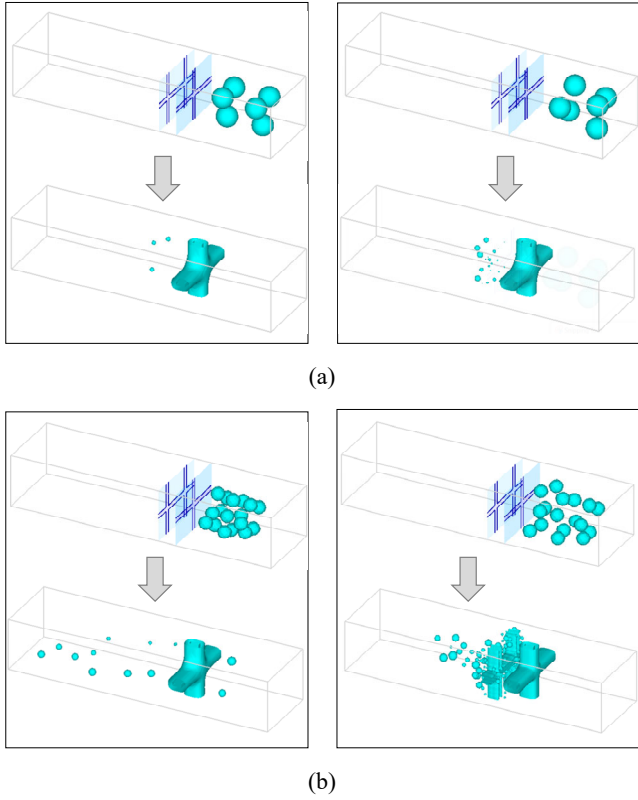
4.3 Effect of volume fraction on the oleophilic-hydrophobic filters efficiency

The efficiency of oil-water separation is also considerably affected by the volume fraction. In the previous Subsection 4.1, to obtain a constant flux, the volume fraction $\phi_i = 5.1\%$ remained constant for the varying droplet sizes. The volume fraction was evaluated as the ratio of volume of the suspended phase (oil droplets) to the volume of the suspending phase (water) in the portion prior to the filter. Essentially, the following equation is given:

$$\phi_i = \frac{V_o}{V_w}, \tag{14}$$

where V_o is the oil droplet volume and V_w is the water volume.

V_o can be modified by adjusting the droplet quantity or the droplet size. The radius remains fixed $R_{d-s} = 0.16$ and the quantity of the droplets is modified to obtain a variety of oil droplet volumes (V_o).

A range of volume fraction $\phi_i = 0.9\% - 4.3\%$ for droplet radius of $R_{d-s} = 0.16$ is used in this simulation to analyse the effects of the volume fraction variance on the performance of superoleophilic/superhydrophobic filter types.

It can be observed from Figure 10(a) that as the volume fraction decreases, the oil-water separation efficiency decreases from 98% to 54%. O/W emulsion density is

influenced significantly by the volume fraction. As the volume fraction increases, a higher amount of oil droplets becomes available within the emulsion resulting in greater droplet affinity towards the contact surface area and more attachment to the oleophilic filter wall. Ultimately, improved oil-water separation efficiency can be achieved (Kang et al., 2020; Zhang et al., 2022).

Although the range $\phi_i = 0.9\% - 4.3\%$ of volume fraction for dimensionless droplet radius correlates to the lowest and highest possible efficiencies, respectively, the efficiency due to the volume fraction possesses extreme value limits. Through simulation, we determined the highest and lowest extremes of the volume fraction is it relates to efficiency. At the high end, $\phi_i = 17\%$, the droplets amalgamate into one large droplet and the simulation ceases as shown in Figure 10(b). Comparatively, the lower limit $\phi_i = 0.9\%$ is obtained by using two droplets with this specific radius, and a volume fraction below this value cannot be achieved due to limitations of the model.

Figure 10   (a) The effect of oil volume fraction on the superoleophilic/superhydrophobic filter efficiency (b) Illustration of droplets behaviour for high volume fraction, $\phi_i = 17\%$ (see online version for colours)

(a)

(b)
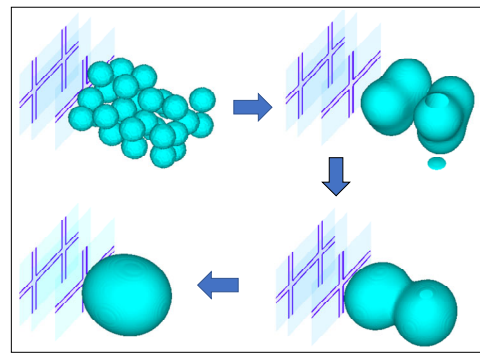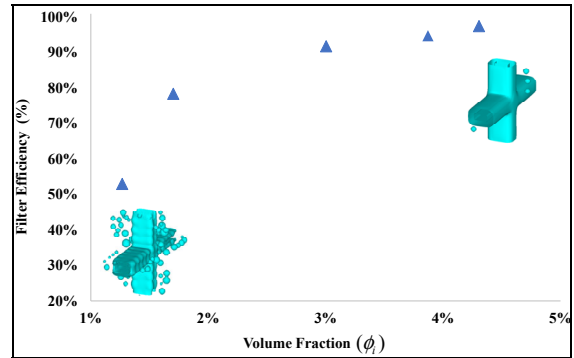
5   Conclusions

A 3D colour-gradient LBM with multi-physics capabilities is applied for the investigation of oleophilic-hydrophobic filters that can be used for oil-water separation. Numerous parameters are employed in this simulation, namely droplet size variance, spatial distribution, and volume fraction.

No researchers to date have applied LBM in the analysis of superoleophilic/superhydrophobic filtration systems. The lack of substantial research created an opportunity for us to use our newly developed 3D model colour-gradient hybrid quasi-steady thermal Lattice-Boltzmann model to evaluate the superoleophilic/superhydrophobic filtration of emulsions.

The use of this LBM model presents the innovative opportunity of designing improved super-wetting filters by mimicking the super-wetting filter system with any desired contact angle and having the ability to modify and validate wetting parameters accordingly. A key advantage of using the LBM numerical model is highlighting the mechanisms that take place in the filtration process which lead to high efficiencies such as the suspended phase adhesion behaviour, its coalescence, and break-up.

The simulation results reveal that the oleophilic-hydrophobic filter type is a suitable method for oil-water separation in stable emulsions, wherein an efficiency as high as 98.7% can be reached in some cases.

The findings show that positive correlations exist between the oleophilic-hydrophobic filter efficiency and the droplet size, droplet spatial distribution, and volume fraction.

Enhancing the oil-water separation performance using oleophilic-hydrophobic filters can be achieved by enlarging the oil droplets in the O/W emulsion during emulsification, as well as increasing the volume fraction. Additionally, decreasing the droplets' scattering rate, or increasing the droplet spatial distribution, will contribute to enhanced oil-water separation performance.

Acknowledgements

References

Al-Tamimi, L., Farhat, H. and Hasan, W.F. (2021) 'Hybrid quasi-steady thermal lattice Boltzmann model for investigating the effects of thermal, surfactants and contact angle on the flow characteristics of oil in water emulsions between two parallel plates', *Journal of Petroleum Science and Engineering*, Vol. 204, p.108572 [online] https://doi.org/10.1016/j.petrol.2021.108572.

Bothamley, M. (2013) 'Gas/liquids separators: quantifying separation performance – part 2', *Oil and Gas Facilities*, Vol. 2, No. 5, pp.35–47 [online] https://doi.org/10.2118/1013-0035-ogf.

Cai, X., Chen, J., Liu, M., Ji, Y. and An, S. (2017) 'Numerical studies on dynamic characteristics of oil-water separation in loop flotation column using a population balance model', *Separation and Purification Technology*, Vol. 176, pp.134–144 [online] https://doi.org/10.1016/j.seppur.2016.12.002.

D'Ortona, U., Salin, D., Cieplak, M., Rybka, R.B. and Banavar, J.R. (1995) 'Two-color nonlinear Boltzmann cellular automata: surface tension and wetting', *Physical Review E*, Vol. 51, No. 4, pp.3718–3728 [online] https://doi.org/10.1103/physreve.51.3718.

Darvishi, M. and Foroutan, M. (2016) 'Molecular investigation of oil-water separation using PVDF polymer by molecular dynamic simulation', *RSC Advances*, Vol. 6, No. 78, pp.74124–74134 [online] https://doi.org/10.1039/c6ra11834h.

Delplace, F. (2018) 'Laminar flow of Newtonian liquids in ducts of rectangular cross-section a model for both physics and mathematics', *Open Access Journal of Mathematical and Theoretical Physics*, Vol. 1, No. 5, pp.198–201 [online] https://doi.org/10.15406/oajmtp.2018.01.00034.

Fan, X. (2016) 'Oil-water separation efficiency and fluid mechanics of a hydrocyclone', *Proceedings of the 2016 7th International Conference on Mechatronics, Control and Materials (ICMCM 2016)* [online] https://doi.org/10.2991/icmcm-16.2016.38.

Farhat, H., Celiker, F., Singh, T. and Lee, J.S. (2011) 'A hybrid lattice Boltzmann model for surfactant-covered droplets', *Soft Matter*, Vol. 7, No. 5, pp.1968–1985 [online] https://doi.org/10.1039/C0SM00569J.

Farhat, H., Lee, J.S. and Kondaraju, S. (2014) 'Suppressing the coalescence in the LBM: colloids rheology', in *Accelerated Lattice Boltzmann Model for Colloidal Suspensions*, pp.99–121, Springer, DOI: 10.1007/978-1-4899-7402-0_5.

Feng, L., Zhang, Z., Mai, Z., Ma, Y., Liu, B., Jiang, L. and Zhu, D. (2004) 'A super-hydrophobic and super-oleophilic coating mesh film for the separation of oil and water', *Angewandte Chemie International Edition*, Vol. 43, No. 15, pp.2012–2014 [online] https://doi.org/10.1002/anie.200353381.

Gavazzoni, C., Silvestrini, M. and Brito, C. (2021) 'Modeling oil-water separation with controlled wetting properties', *The Journal of Chemical Physics*, Vol. 154, No. 10, p.104704 [online] https://doi.org/10.1063/5.0041070.

Halliday, I., Hollis, A.P. and Care, C.M. (2007) 'Lattice Boltzmann algorithm for continuum multicomponent flow', *Physical Review E*, Vol. 76, No. 2 [online] https://doi.org/10.1103/physreve.76.026708.

Hou, B., Jia, R., Fu, M., Wang, Y., Bai, Y. and Huang, Y. (2018) 'Wettability alteration of an oil-wet sandstone surface by synergistic adsorption/desorption of cationic/nonionic surfactant mixtures', *Energy & Fuels*, Vol. 32, No. 12, pp.12462–12468, DOI: 10.1021/acs.energyfuels.8b03450.

Jiang, S., Meng, X., Chen, B., Wang, N. and Chen, G. (2020) 'Electrospinning superhydrophobic-superoleophilic PVDF-SiO$_2$ nanofibers membrane for oil-water separation', *Journal of Applied Polymer Science*, Vol. 137, No. 47, p.49546 [online] https://doi.org/10.1002/app.49546.

Ju, J., Wang, T. and Wang, Q. (2015) 'A facile approach in fabricating superhydrophobic and superoleophilic poly (vinylidene fluoride) membranes for efficient water-oil separation', *Journal of Applied Polymer Science*, Vol. 132, No. 24 [online] https://doi.org/10.1002/app.42077.

Kang, W., Kang, X., Yang, H., Gebremariam, H. and Li, Z. (2020) 'Efficient oil removal of polymer flooding produced sewerage using superhydrophobic mesh filtration method', *Colloids and Interfaces*, Vol. 4, No. 3, p.32 [online] https://doi.org/10.3390/colloids4030032.

Martys, N.S. and Chen, H. (1996) 'Simulation of multicomponent fluids in complex three-dimensional geometries by the lattice Boltzmann method', *Physical Review E*, Vol. 53, No. 1, p.743 [online] https://doi.org/10.1103/PhysRevE.53.743.

Mehanna, Y.A. and Crick, C.R. (2020) 'Heat-treated micronized polyethylene powder for efficient oil/water separating filters', *Materials*, Vol. 13, No. 14, p.3160 [online] https://doi.org/10.3390/ma13143160.

Mino, Y., Hasegawa, A., Shinto, H. and Matsuyama, H. (2018) 'Lattice-boltzmann flow simulation of an oil-in-water emulsion through a coalescing filter: effects of filter structure', *Chemical Engineering Science*, Vol. 177, pp.210–217 [online] https://doi.org/10.1016/j.ces.2017.11.027.

Oshinowo, L.M., Quintero, C.G. and Vilagines, R.D. (2015) 'CFD and population balance modeling of crude oil emulsions in batch gravity separation – comparison to ultrasound experiments', *Journal of Dispersion Science and Technology*, Vol. 37, No. 5, pp.665–675 [online] https://doi.org/10.1080/01932691.2015.1054508.

Padaki, M., Surya Murali, R., Abdullah, M.S., Misdan, N., Moslehyani, A. and Ismail, A.F. (2015) 'Membrane technology enhancement in oil-water separation. A review', *Desalination*, Vol. 357, pp.197–207 [online] https://doi.org/10.1016/j.desal.2014.11.023.

Rasouli, S., Rezaei, N. and Hamedi, H. (2021) 'Superhydrophobic and superoleophilic membranes for oil-water separation application: a comprehensive review', *Materials & Design*, Vol. 204, No. 109599 [online] https://doi.org/10.1016/j.matdes.2021.109599.

Sadler, E. and Crick, C.R. (2021) 'Suction or gravity-fed oil-water separation using PDMS-coated glass filters', *Sustainable Materials and Technologies*, Vol. 29 [online] https://doi.org/10.1016/j.susmat.2021.e00321.

Shang, Y., Si, Y., Raza, A., Yang, L., Mao, X., Ding, B. and Yu, J. (2012) 'An in situ polymerization approach for the synthesis of superhydrophobic and superoleophilic nanofibrous membranes for oil-water separation', *Nanoscale*, Vol. 4, No. 24, p.7847 [online] https://doi.org/10.1039/c2nr33063f.

Singh, C.J., Mukhopadhyay, S. and Rengasamy, R.S. (2021) 'Oil separation from oil in water emulsion by coalescence filtration using kapok fibre', *Environmental Technology*, pp.1–13 [online] https://doi.org/10.1080/09593330.2021.1972168.

Tu, C-W., Tsai, C-H., Wang, C-F., Kuo, S-W. and Chang, F-C. (2007) 'Fabrication of superhydrophobic and superoleophilic polystyrene surfaces by a facile one-step method', *Macromolecular Rapid Communications*, Vol. 28, No. 23, pp.2262–2266 [online] https://doi.org/10.1002/marc.200700447.

Varnik, F., Truman, P., Wu, B., Uhlmann, P., Raabe, D. and Stamm, M. (2008) 'Wetting gradient induced separation of emulsions: a combined experimental and lattice Boltzmann computer simulation study', *Physics of Fluids*, Vol. 20, No. 7, p.72104 [online] https://doi.org/10.1063/1.2963958.

Wang, C., Yao, T., Wu, J., Ma, C., Fan, Z., Wang, Z., Cheng, Y., Lin, Q. and Yang, B. (2009) 'Facile approach in fabricating superhydrophobic and superoleophilic surface for water and oil mixture separation', *ACS Applied Materials & Interfaces*, Vol. 1, No. 11, pp.2613–2617 [online] https://doi.org/10.1021/am900520z.

Woo, S., Park, H.R., Park, J., Yi, J. and Hwang, W. (2020) 'Robust and continuous oil/water separation with superhydrophobic glass microfiber membrane by vertical polymerization under harsh conditions', *Scientific Reports*, Vol. 10, No. 1 [online] https://doi.org/10.1038/s41598-020-78271-9.

Wu, J., Xie, A., Yang, J., Dai, J., Li, C., Yan, Y. and Cui, J. (2020) 'A facile surface modification of a PVDF membrane via CaCO$_3$ mineralization for efficient oil/water emulsion separation', *New Journal of Chemistry*, Vol. 44, No. 48, pp.20999–21006 [online] https://doi.org/10.1039/d0nj03329d.

Zhang, J., He, Y.-t., Liu, S. and Xu, J.-y. (2022) 'Oil-water separation in a cylindrical cyclone with vortex finder', *Physics of Fluids*, Vol. 34, No. 3, p.33314 [online] https://doi.org/10.1063/5.0085029.

Zhang, W., Shi, Z., Zhang, F., Liu, X., Jin, J. and Jiang, L. (2013) 'Superhydrophobic and superoleophilic PVDF membranes for effective separation of water-in-oil emulsions with high flux', *Advanced Materials*, Vol. 25, No. 14, pp.2071–2076 [online] https://doi.org/10.1002/adma.201204520.

Nomenclature

B_0	Bond number
c_i	Lattice velocity
c_s	Speed of sound
D_{ifs}	Thermal diffusivity
D_s	Diffusion coefficient
E_0	Elasticity of surfactant
e_i	Lattice link
$\widehat{f}_i^q$	Post-collision equilibrium distribution function
F	Constant pressure per unit length
f^q	Collision density distribution function
h	Channel height
lf	Lattice force
lu	Lattice spatial unit
P	Undisturbed flow power
Q	Volume flow rate
R_{ch}	Channel radius
R_{d-s}	Droplet diameter
R_P	Power number ratio
T	Temperature
T_0	Reference temperature
$\bar{U}$	Average velocity
u	Fluid velocity
U_0	Central velocity
v	Kinematic viscosity

Nomenclature (continued)

Greek symbols	
ϕ_i	Volume fraction
γ	Interferential tension
Δp	Pressure difference
δ_t	Lattice time step
θ	Contact angle
θ_d	Temperature dependent contact angle
λ	Physical relaxation time
μ	Dynamic viscosity
ξ	Macroscopic physical velocity
ρ	Macroscopic density
ρN	Phase field
σ	Surface tension
$\sigma 0$	Clean droplet surface tension
τ	Lattice relaxation time
φ	Flow viscous dissipation
ωi	LBM weighting constants
Subscripts	
AD	Adhesion force
B	Blue fluid
d	Droplet
LV	Liquid-vapour
N	Normalised
R	Red fluid
Ref	Reference
SV	Solid-vapour
Superscripts	
e	Emulsion
eq	Equilibrium
G_{ads}^{σ}	Fluid-solid adhesion force constant
H	Heavy fluid
K	Interface curvature
L	Light fluid
o	Oil
T	Temperature dependent
w	Water
Γ	Surfactant concentration
Γ^*	Dimensionless surfactants concentration
Γ_{∞}	Saturation surfactant concentration
$\dot{\gamma}$	Shear strain rate